JOC The Journal of Organic Chemistry

Article

pubs.acs.org/joc

π-Extended Thiadiazoles Fused with Thienopyrrole or Indole Moieties: Synthesis, Structures, and Properties

Shin-ichiro Kato,[†] Takayuki Furuya,[†] Atsushi Kobayashi,[†] Masashi Nitani,[‡] Yutaka Ie,[‡,§] Yoshio Aso,[‡] Toshitada Yoshihara,[†] Seiji Tobita,[†] and Yosuke Nakamura*[,†]

[†]Department of Chemistry and Chemical Biology, Graduate School of Engineering, Gunma University, 1-5-1 Tenjin-cho, Kiryu, Gunma 376-8515, Japan

[‡]The Institute of Scientific and Industrial Research (ISIR), Osaka University, 8-1 Mihogaoka, Ibaraki, Osaka 567-0047, Japan

[§]PRESTO-JST, 4-1-8 Honcho, Kawaguchi, Saitama 333-0012, Japan

Supporting Information

ABSTRACT: We report the syntheses, structures, photophysical properties, and redox characteristics of donor−acceptor-fused π-systems, namely π-extended thiadiazoles **1**−**5** fused with thienopyrrole or indole moieties. They were synthesized by the Stille coupling reactions followed by the PPh_3-mediated reductive cyclizations as key steps. X-Ray crystallographic studies showed that isomeric **1b** and **2b** form significantly different packing from each other, and **1a** and **4a** afford supramolecular networks via multiple hydrogen bonding with water molecules. Thienopyrrole-fused compounds **1b** and **2b** displayed bathochromically shifted intramolecular charge-transfer (CT) bands and low oxidation potentials as compared to indole-fused analog **3b** and showed moderate to good fluorescence quantum yields (Φ_f) up to 0.73. In **3b**−**5b**, the introduction of electron-donating substituents in the indole moieties substantially shifts the intramolecular CT absorption maxima bathochromically and leads to the elevation of the HOMO levels. The Φ_f values of **3**−**5** (0.04−0.50) were found to be significantly dependent on the substituents in the indole moieties. The OFET properties with **1b** and **2b** as an active layer were also disclosed.

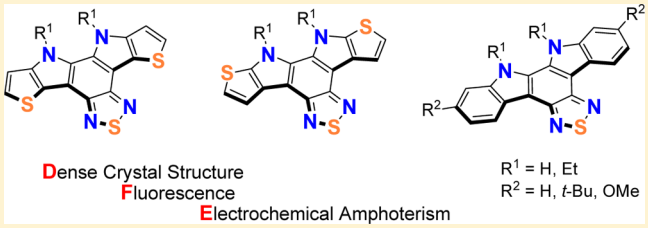

INTRODUCTION

The development of organic π-conjugated molecules for organic electronics, such as organic light-emitting diodes (OLEDs), organic field-effect transistors (OFETs), and organic photovoltaics (OPVs), remains a key objective.[1,2] Organic materials have distinct advantage of their structural diversity, which can be achieved by versatile synthetic protocols in organic chemistry. It is important to tailor the electronic structure of π-conjugated molecules and control the solid-state structure to obtain appropriate intermolecular interactions in an intelligent way. Consequently, recent advances in exploring π-conjugated molecules involve the development of multifused aromatic and heteroaromatic compounds, because it is expected that their flat and rigid frameworks provide the effective extension of π-conjugation and allow for forming a dense molecular packing and thereby, lead to spectacular properties such as strong fluorescence and high carrier mobility. Over the years, polycyclic aromatic hydrocarbons (PAHs), such as acene derivatives with collinearly fused benzene rings and 2D extended fully fused compounds, were extensively studied.[3,4] Thienoacenes[5] and azaacenes[6,7] have been also synthesized, and the effects of the replacement of benzene rings in acenes with thiophene and pyrazine rings on the optical and electronic properties have been discussed. Furthermore, various ladder-type π-conjugated systems incorporating heteroatoms,[8] such as nitrogen,[9] silicon,[10] and boron,[11] have been synthesized, and their potential applications as π-functional materials have been recently investigated by taking advantage of the characteristic electronic properties derived from heteroatoms.

Intramolecular charge-transfer (CT) interactions are a fundamental property of π-systems consisting of strong electron donors (D) and acceptors (A) connected via a π-spacer.[12] Donor−acceptor-substituted compounds have a potential to possess the small HOMO−LUMO gap and show the electrochemically amphoteric behavior, and thereby they are of current interest as attractive materials.[13] Therefore, the D−A-fused heterocycles would be also an interesting class of π-electronic systems. In addition to the prominent features of the D−A-substituted compounds, they are expected to form densely packed structures in the solid state due to the multifused π-framework. As for D−A-fused molecules, Yamashita and co-workers synthesized tetrathiafulvalene (TTF)−quinoxaline-fused systems and demonstrated their considerably high stability and good carrier mobility.[14] Liu and co-workers extensively studied analogous compounds, which resulted from fusing TTF and strong acceptors, such as phenazine and perylenebisimide units.[15] Very recently, Xiao

Received: July 11, 2012
Published: August 8, 2012

and co-workers have synthesized carbazole−perylenebisimide-fused derivatives and disclosed the remarkable third-order nonlinear susceptibility reflecting the intramolecular CT interactions.[16] Siri and co-workers[17] and Miao and co-workers[18] independently reported the efficient synthetic pathways of dihydrotetraazapentacenes, namely dihydrophenazine−quinoxaline-fused molecules, as interesting D−A-fused heterocycles without exocyclic double bond, and their optoelectronic and electrochemical properties and solid-state structures were studied.

It is likely that the choice of building blocks in the molecular design of the D−A-fused systems is critical because they are anticipated to dominate the properties in many cases. Benzothiadiazole (BTD) unit is a leading candidate as a strong electron-acceptor and an important component of narrow band gap π-conjugated oligomers and copolymers for organic solar cells.[19] The BTD unit has been combined with carbazoles, fluorenes, pyrroles, thiophenes, and other electron-rich building blocks.[20] Hence, we became interested in π-extended thiadiazoles **1** and **2** fused with thienopyrrole moieties and thiadiazoles **3**−**5** fused with indole moieties (Chart 1). We

Chart 1

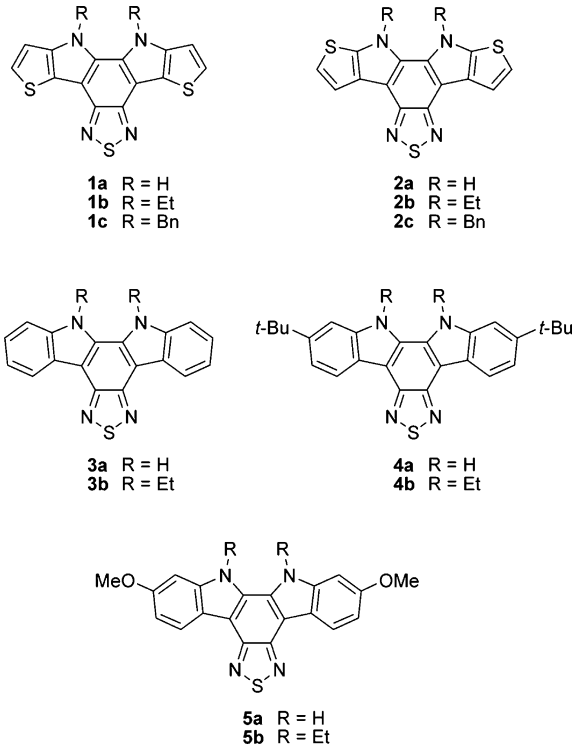

envisaged that the ring fusion of highly electron-donating thienopyrrole or indole moieties to an electron-accepting BTD unit brings about not only the intramolecular CT interactions but also the efficient intermolecular interactions in the solid state.[21] Very recently, Cheng and Hsu's group independently reported the synthesis of **1a**.[21g,22] A few thiadiazole derivatives fused with indole moieties were sporadically reported;[21b,f] however, the elucidation of the structure−property relationships still remain to give the guideline for the molecular design of the D−A-fused systems as π-functional materials. Here we report the synthesis of **1**−**5** by the alternative synthetic method and their structure−property relationships in detail. The electronic properties were systematically investigated by means of electronic absorption spectroscopy, cyclic voltammetry (CV), and theoretical calculations. The photophysical properties were further elucidated by fluorescence spectroscopy, fluorescence lifetime measurements, and time-resolved photoacoustic measurements. The X-ray crystallographic structures of **1a**, **1b**, **2b**, **4a**, and **5b** were determined and examined in detail. The p-type semiconducting nature of **1b** and **2b** was also disclosed.

RESULTS AND DISCUSSION

Synthesis. The synthetic route to **1**−**5** is outlined in Scheme 1. First, we subjected **6** to Stille coupling reaction with tributyl(2-thienyl)tin to prepare **7**.[23] Then, we carried out double-reductive cyclization of **7** with PPh_3 in *o*-dichlorobenzene (*o*-DCB) at the refluxing temperature[24] and isolated **1a** in a remarkably high yield of 97%. This result prompted us to synthesize isomeric compound **2a**. Using **8** as a precursor which was synthesized by Stille coupling of **6** with tributyl(3-thienyl)tin, the double cyclization with PPh_3 proceeded smoothly, and noticeably **2a** was obtained as the sole product in a yield of 93%. We next examined the synthesis of indole analogs **3a**−**5a** with H-, *t*-Bu-, and OMe-substituents, respectively, by the PPh_3-mediated reductive cyclization reactions. As a result, the reactions of **9**−**11** with PPh_3 in *o*-DCB at the refluxing temperature furnished the desired **3a**−**5a** in 97%, 70%, and 92% yields, respectively. It was recently reported that **3a**[21b] and **5a**[21f] were prepared by $P(OEt)_3$-mediated reactions in 51% and 61%, respectively (Supplementary Scheme S1 in the Supporting Information). Overall, the reactions with PPh_3 appear to give better yields than those with $P(OEt)_3$, and the yields were readily reproducible.[24b] In most cases, almost the only byproduct, triphenylphosphine oxide, was easily removed by standard chromatography and/or washing with appropriate solvents. We also attempted the cyclization reaction of 4,7-di(2-furyl)-5,6-dinitro-2,1,3-benzothiadiazole by the treatment with PPh_3, however, only decomposed materials were recovered presumably due to instability of the cyclized product (Supplementary Scheme S2). *N*-Ethyl products **1b**−**5b** were readily obtained by the reaction of the corresponding **1a**−**5a** with iodoethane in the presence of NaOH as a base in DMF. Compounds **1b**−**5b** are more soluble than **1a**−**5a**, respectively, in common organic solvents without the loss of the tendency for crystallization upon introduction of the ethyl groups. Compounds **1a** and **2a** were also converted to *N*-benzyl products **1c** and **2c**, respectively. *N*-Benzylation of **3a**−**5a** was not investigated on the basis of the results that the photophysical and electrochemical properties of **1c** and **2c** are not significantly different from those of **1b** and **2b**, respectively (*vide infra*). All compounds were fully characterized by various spectroscopic methods.

Structural Properties. We determined the molecular structures by X-ray analysis of single crystals of **1a**, **1b**, **2b**, **4a**, and **5b**. Single crystals suitable for X-ray diffraction analysis were obtained by slow diffusion of hexane into a solution of the molecules in CH_2Cl_2 or acetone. Extensive X-ray analyses confirmed that all of the π-extended thiadiazoles have highly planar frameworks (Figure 1). Especially, the planarity of **1a** and **4a** is still high relative to that of **1b**, **2b**, and **5b**, in which the steric hindrance between the ethyl groups on the nitrogen atoms occurs. In all the molecular structures in the solid state, no noticeable bond-length alternation is observed and the bond angles are inconspicuous.

dx.doi.org/10.1021/jo301458m | J. Org. Chem. 2012, 77, 7595−7606

Scheme 1. Synthesis of π-Extended Thiadiazoles 1−5 Fused with Thienopyrrole or Indole Moieties[a]

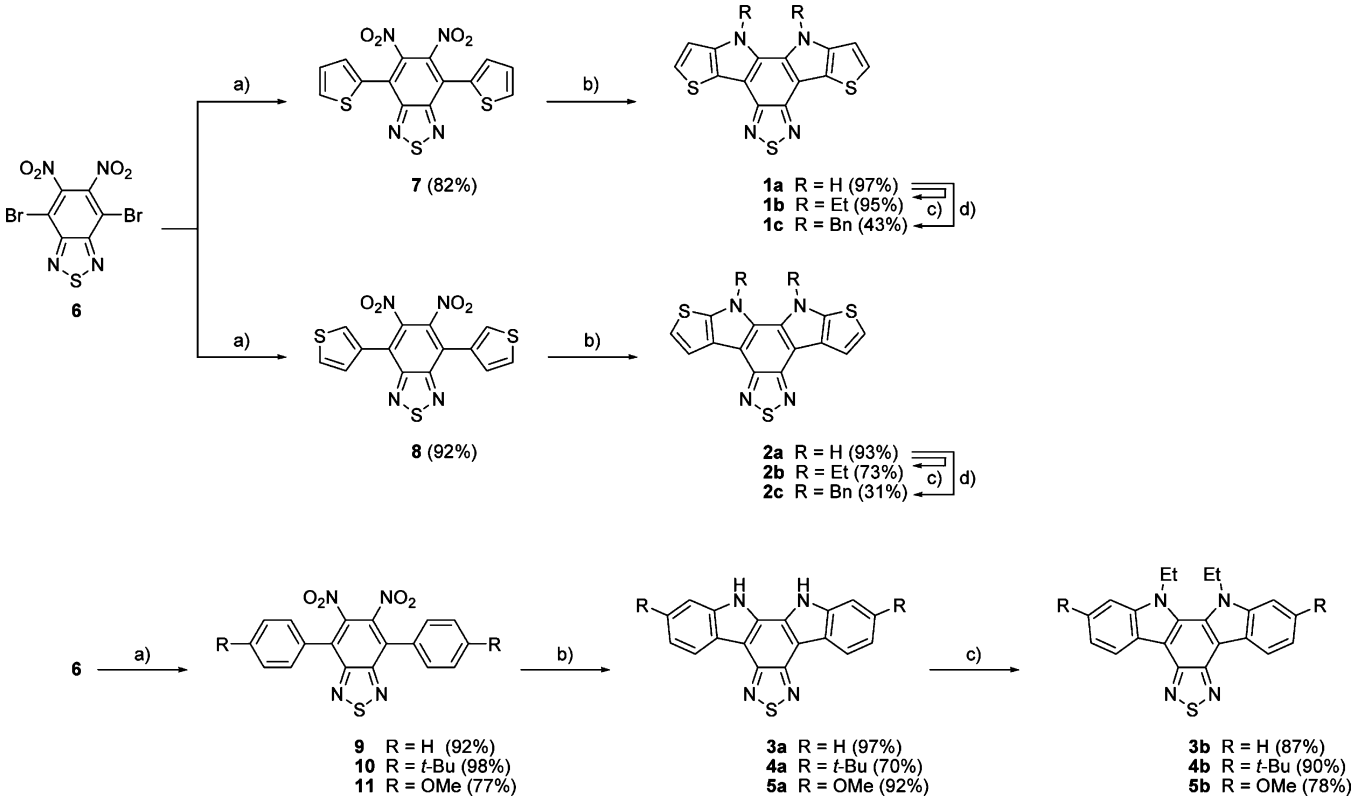

[a]Reagents and conditions: (a) $Pd(PPh_3)_4$, tributyl(2-thienyl)tin for **7**, tributyl(3-thienyl)tin for **8**, tributylphenyltin for **9**, tributyl(4-*tert*-butylphenyl)tin for **10**, and tributyl(4-methoxyphenyl)tin for **11**, THF, reflux. (b) PPh_3, *o*-dichlorobenzene (*o*-DCB), reflux. (c) Iodoethane, NaOH, DMF, 50 °C. (d) benzyl bromide, NaOH, DMF, 60 °C.

For the potential usefulness of π-conjugated molecules in organic electronics, the π-stacking motif with large overlap of π-orbitals with the neighboring molecules in the solid state is a critical aspect. As shown in Figure 2a and b, isomeric **1b** and **2b** exhibit good $\pi-\pi$ stacking with a distance of about 3.35−3.4 Å, however, they differ much in the packing motif reflecting the structural difference. Compound **1b** is packed in a head-to-tail manner to form a 1D column in a parallel and slanted arrangement and the columns assemble together by weak S···H interactions with a distance of 2.84 Å to give a sheet-like network (Figure 2a). The thienopyrrole moieties are overlapped with the BTD moieties, suggesting the presence of intermolecular CT interactions between the thienopyrrole donor and BTD acceptor parts. On the other hand, **2b** forms a stacked dimer structure with a close C···C distance of 3.36 Å, which is aligned in a 1D array by efficient S···S interactions with a distance of 3.59 Å (Figure 2b). Again, the dimer is packed in a sandwich-herringbone motif by C−H···π interactions. Compound **5b** forms offset stacks in the single crystal with a longer distance of 3.49 Å than those in the crystals of **1b** and **2b**, and a brickwork motif runs parallel to the *b*,*c* plane (Supplementary Figure S1, Supporting Information).

Interestingly, the water molecules, which apparently came from the solvent of wet acetone, were included in the single crystals of both **1a** and **4a** in a 1:1 stoichiometry, whereas the crystals of **1b**, **2b**, and **5b** with the Et-substituents described above did not contain solvent molecules. As shown in Figures 3 and 4, both **1a** and **4a** interact with water molecules through a combination of N−H···O, C═N···H, and O−H···π interactions, which led to the formation of supramolecular networks. Thus, in the crystal packing of **1a**, the indole sites prefer to trap the water molecules by bifurcated N−H···O hydrogen bonding (2.05 and 2.26 Å), and the neighboring molecules interact with the water molecules by C═N···H hydrogen bonding with the thiadiazole sites (2.04 Å). The electron-rich pyrrole rings are also involved in favorable O−H···π interactions. Likewise, in the crystal of **4a**, the combination of the N−H···O hydrogen bonding (2.38 and 1.94 Å) between the water molecules and the indole sites and the C═N···H hydrogen bonding between the water and the thiadiazole sites yields a sheet-like structure (Figure 4a). The sheets are assembled in a brickwork motif through the combination of O−H···π (2.40 and 2.45 Å) and $\pi\cdots\pi$ interactions (Figure 4b). It is noteworthy that both **1a** and **4a** accommodate the water molecules without losing the efficient S···π and/or $\pi\cdots\pi$ interactions.

Photophysical Properties. To investigate the photophysical properties in detail, we measured the UV−vis and fluorescence spectra of **1**−**5** in various solvents, and the representative data are summarized in Table 1. These data are mainly discussed from the viewpoints of (1) the effect of the orientation of fused heterorings in **1a**−**c** and **2a**−**c** and (2) the effect of the substituents in indole moieties in **3a**,**b**−**5a**,**b**.

Figure 5a shows the UV−vis spectra of compounds **1b**−**5b** in CH_2Cl_2. The spectra of **1a**−**c** and **2a**−**c** feature broad CT absorptions of moderate intensity ($\varepsilon \approx 5000-7000\ M^{-1}\ cm^{-1}$) with the longest absorption maxima (λ_{max}^{abs}) between 415 and 436 nm in CH_2Cl_2 (Supplementary Figure S2 and S3 and Table S1 and S2, Supporting Information). Introduction of the ethyl or benzyl groups on the nitrogen atoms in **1b**,**c** and **2b**,**c** results in slightly bathochromic shifts of the λ_{max}^{abs} values as compared

dx.doi.org/10.1021/jo301458m | J. Org. Chem. 2012, 77, 7595−7606

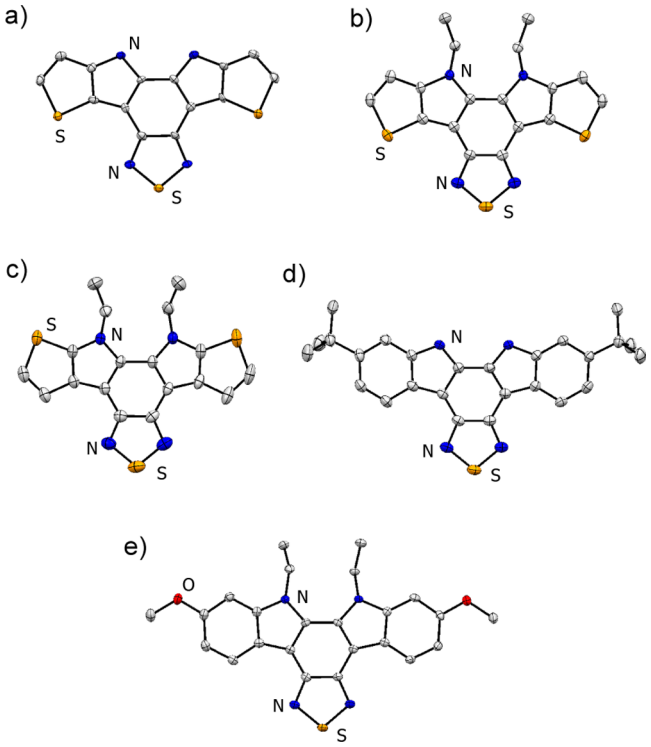

Figure 1. ORTEP plots of (a) **1a**, (b) **1b**, (c) **2b**, (d) **4a**, and (e) **5b** with displacement ellipsoids at the 50% probability level. Water molecules in the crystals of **1a** and **4a**, and H-atoms are omitted for clarity.

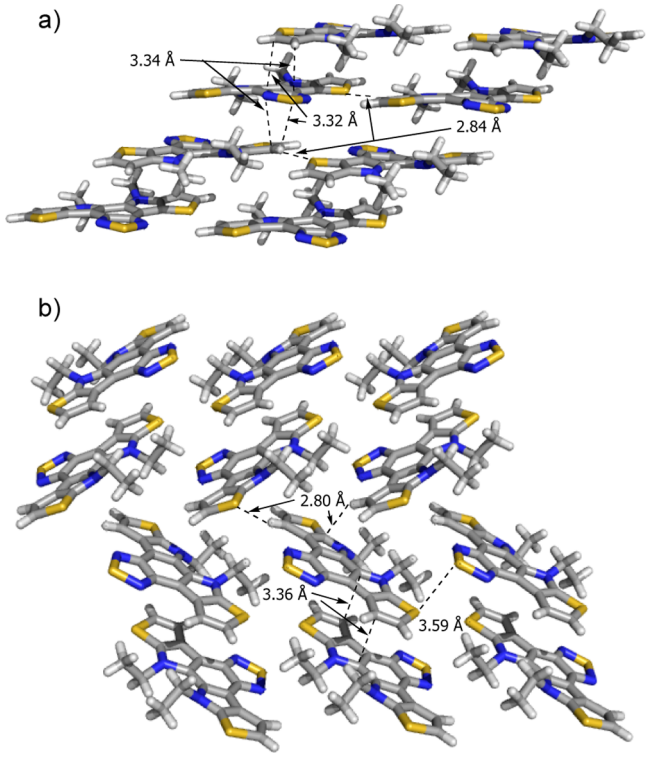

Figure 2. Arrangement of neighboring molecules in the crystal packing of (a) **1b** and (b) **2b**.

to **1a** and **2a**, respectively. For example, **1a** shows the λ_{max}^{abs} value of 423 nm (ε = 5800 M^{-1} cm^{-1}), while **1b** and **1c** feature the λ_{max}^{abs} values of 436 nm (ε = 7100 M^{-1} cm^{-1}) and 434 nm

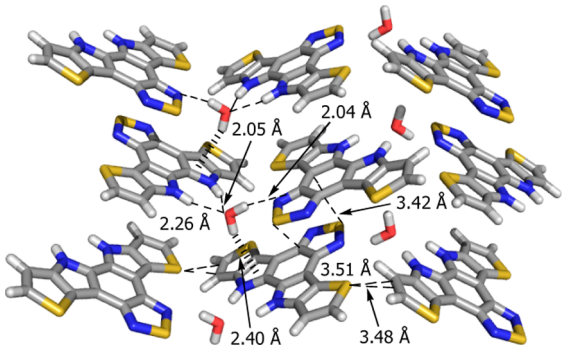

Figure 3. Arrangement of neighboring molecules in the crystal packing of **1a**.

(ε = 6200 M^{-1} cm^{-1}), respectively. Similar bathochromic shifts are observed when going from **2a** (λ_{max}^{abs} = 415 nm, ε = 5100 M^{-1} cm^{-1}) to **2b** (λ_{max}^{abs} = 425 nm, ε = 7000 M^{-1} cm^{-1}) and **2c** (λ_{max}^{abs} = 424 nm, ε = 6400 M^{-1} cm^{-1}). The λ_{max}^{abs} values and the absorption edges of **1a**−**c** are slightly red-shifted by about 10 nm as compared to those of the corresponding **2a**−**c**. According to the density functional theory (DFT) calculations (B3LYP/6-311G**//B3LYP/6-31G*) by the Gaussian 03 suit of program,[25] **1b** has a larger dipole moment of 2.608 D than that for **2b** to be 2.053 D, which may account for the difference of the λ_{max}^{abs} values between **1a**−**c** and **2a**−**c**.[26] The broad bands of **1a**−**c** in the region of 400−500 nm are quite similar to those of **2a**−**c**, whereas the absorption curves in the region of 300−350 nm significantly differ from each other.

To investigate the solvent effects on the photophysical properties, we measured the UV−vis and fluorescence spectra in various media from nonpolar to polar solvents.[27] While the UV−vis spectra of **1a**−**c** and **2a**−**c** are slightly changed between nonpolar toluene and polar DMF, remarkable fluorescence solvatochromism for **1a**−**c** and **2a**−**c** was observed depending on the polarity of the solvents. The color of fluorescence varies from green in toluene to yellow in DMF (Supplementary Figure S4, Supporting Information). Figure 5b shows the fluorescence spectra of **2b** in different solvents as a typical example. Upon increasing the solvent polarity from toluene to DMF,[28] the fluorescence maxima (λ_{max}^{fl}) of **2b** shift to longer wavelength region by 44 nm: 508 nm in toluene and 552 nm in DMF (see Supplementary Figure S5−S10 for **1a**−**c** and **2a**−**c**). The observed solvatochromic effects in the emission strongly suggest a more polar electronic structure in the excited state than in the ground state in **1a**−**c** and **2a**−**c** upon the intramolecular CT interactions. We determined the absolute fluorescence quantum yields (Φ_f) of **1a,b** and **2a,b** in various solvents by using an integrating sphere system.[29] In nonpolar toluene, THF, and ethyl acetate, the Φ_f values of **1a,b** are almost 1.5 times as high as those of the corresponding **2a,b**: 0.68 (**1a**), 0.73 (**1b**), 0.42 (**2a**), and 0.45 (**2b**) in toluene. On the contrary, in CH_2Cl_2 and polar DMF, the Φ_f values of **1a,b** are almost the same as those of the corresponding **2a,b**, although the reason for these findings is unclear at present (Table 1, and Supplementary Table S1 and S2).

One peak and one shoulder were observed for **3a,b** over 350 nm in contrast to **1a,b** and **2a,b** which show distinctive two peaks, probably reflecting the structural difference between the indole and thienopyrrole moieties (Figure 5a and Supplementary Figure S11 and S12, Supporting Information). A comparison of **3**−**5** shows the effects of the substituents in the

dx.doi.org/10.1021/jo301458m | J. Org. Chem. 2012, 77, 7595−7606

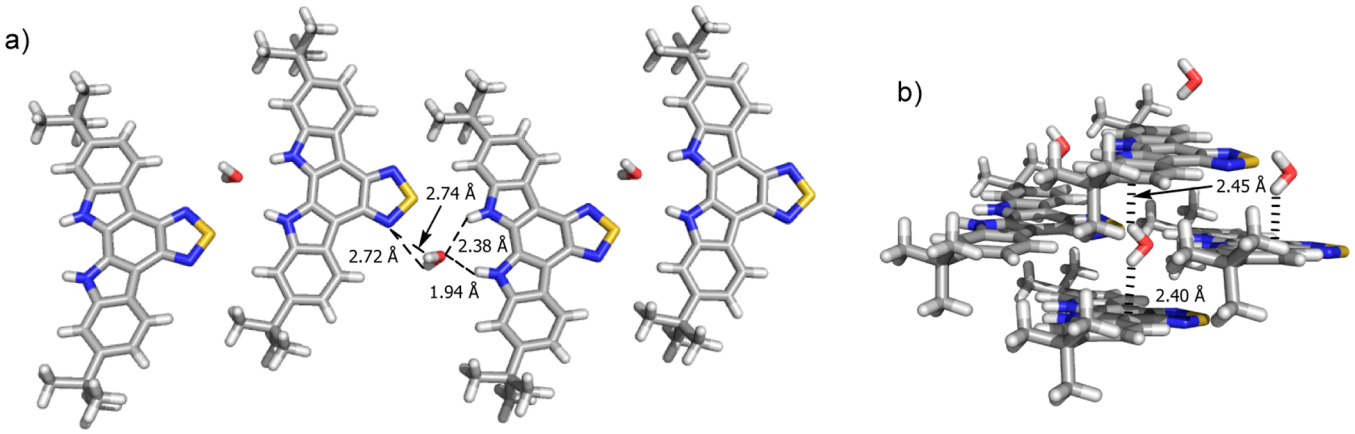

Figure 4. Arrangement of neighboring molecules in the crystal packing of (a) top view and (b) side view of **4a**.

Table 1. Summary of Photophysical Data of 1b−5b[a]

	solv.	λ_{max}^{abs} [nm (eV)][b]	λ_{max}^{fl} [nm]	τ_f [ns][c]	Φ_f[d]	k_r [10^7 s^{-1}][e]	k_{nr} [10^7 s^{-1}][f]
1b	toluene	432 (2.91)	523	19.4	0.73	3.8	1.4
	THF	436 (2.85)	539	23.7	0.68	2.9	1.4
	EtOAc	433 (2.87)	538	24.2	0.63	2.6	1.5
	CH_2Cl_2	436 (2.85)	565	16.6	0.33	2.0	4.0
	DMF	441 (2.82)	573	22.1	0.42	1.9	2.6
2b	toluene	423 (2.94)	508	13.0	0.45	3.5	4.2
	THF	424 (2.93)	521	15.0	0.51	3.4	3.3
	EtOAc	422 (2.94)	521	15.6	0.47	3.0	3.4
	CH_2Cl_2	425 (2.92)	548	14.6	0.34	2.3	4.5
	DMF	430 (2.89)	552	16.8	0.43	2.5	3.4
3b	toluene	420[g] (2.96)	470	0.97	0.07	6.9	96
	CH_2Cl_2	420[g] (2.96)	497	1.00	0.04	4.3	95
	DMF	420[g] (2.96)	500	1.07	0.04	4.1	89
4b	toluene	425[g] (2.92)	489	1.18	0.08	7.0	78
	CH_2Cl_2	430[g] (2.89)	515	1.81	0.07	3.9	51
	DMF	430[g] (2.89)	515	1.57	0.07	4.2	59
5b	toluene	439 (2.83)	517	7.5	0.41	5.5	7.9
	CH_2Cl_2	440 (2.82)	553	12.6	0.44	3.1	4.5
	DMF	445 (2.79)	557	15.3	0.49	3.2	3.3

[a]Complete data for **1**−**5** are included in the Supporting Information. [b]Only the longest absorption maxima are shown. [c]Lifetime. [d]Absolute quantum yields determined by an integrating sphere system. [e]Radiative decay constant. [f]Nonradiative decay constant. [g]Shoulder.

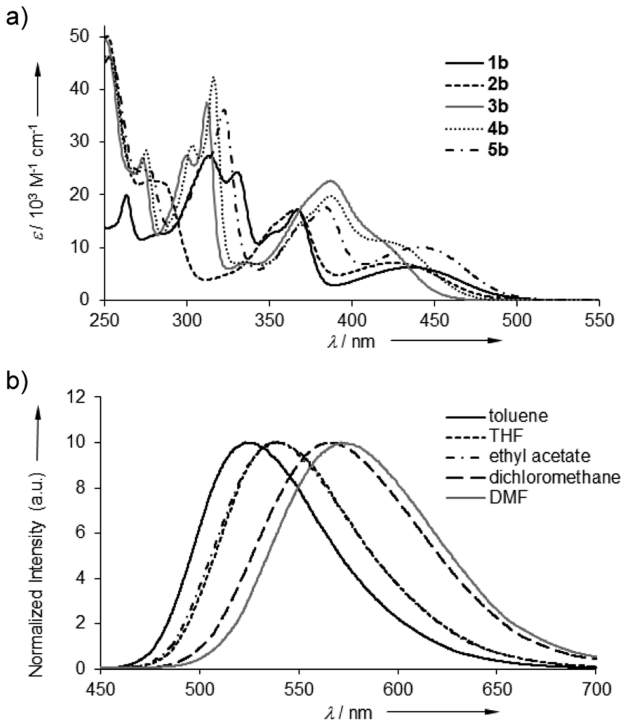

Figure 5. (a) UV−vis absorption spectra of **1b**−**5b** in CH_2Cl_2. (b) Fluorescence spectra of **2b** in different solvents.

indole moieties on the photophysical properties.[30] Introduction of the substituents results in the longer wavelength shifts of both λ_{max}^{abs} and λ_{max}^{fl} (Table 1, Figure 5, and Supplementary Table S3), and thus the λ_{max}^{abs} values for **3b**, **4b**, and **5b** in CH_2Cl_2 were observed at 420, 430, and 440 nm, respectively, as shown in Figure 5a. On the contrary, the absorption maxima of **3**−**5** around 380 nm, which are probably related to the $S_0 \rightarrow S_2$ transitions, are nearly independent of the substituents. The λ_{max}^{fl} values of **3**−**5** follow the trend of their λ_{max}^{abs} values. Thus, as summarized in Table 1, compounds **3b**, **4b**, and **5b** feature the λ_{max}^{fl} values of 497, 515, and 553 nm in CH_2Cl_2, respectively (see Supplementary Table S3 for **3a**−**5a**). As is the case with **1** and **2**, compounds **3**−**5** also exhibited characteristic fluorescence solvatochromism (Supplementary Figure S11−S16). Notably, the Φ_f values were dramatically affected by the substituents. Compounds **5a**,**b** with the OMe-substituents exhibit the Φ_f values of 0.41−0.50 in toluene, CH_2Cl_2, and DMF, which are slightly lower than those of **1a**,**b** and almost comparable to those of **2a**,**b** (Table 1 and Supplementary Table S3). However, **3a**,**b** and **4a**,**b** with the H- and *t*-Bu-substituents, respectively, display unexpectedly low Φ_f values of 0.04−0.12 by about 1 order of magnitude compared to **5a**,**b**.

To gain insight into the photophysical properties of **1**−**5**, we determined their fluorescence lifetimes (τ_f) in various solvents with the time-correlated single-photon counting method (Figure 6), and calculated the radiative (k_r) and nonradiative (k_{nr}) decay rate constants from the singlet excited state,[31] based on the equations of $k_r = \Phi_f/\tau_f$ and $k_{nr} = (1 - \Phi_f)/\tau_f$ (Table 1 and Supplementary Table S1−S3, Supporting Information). Compounds **1a**,**b** exhibit slightly longer τ_f values (14.4−24.2 ns) than those of **2a**,**b** (13.0−16.8 ns). Compounds **1a**,**b** and **2a**,**b** exhibit the similar k_r values in many cases, however, in toluene, THF, and ethyl acetate the k_{nr} values for **1a**,**b** are somewhat smaller than those for **2a**,**b**. These findings correlate with the trend of their Φ_f values as described above.

dx.doi.org/10.1021/jo301458m | J. Org. Chem. 2012, 77, 7595−7606

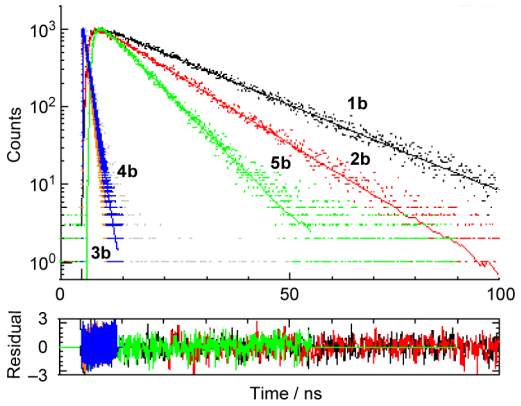

Figure 6. Fluorescence decay curves (top) and residual (bottom) of **1b**−**5b** measured by the time-correlated single-photon counting method.

Compounds **5a**,**b** display the τ_f values of 6.9−16.1 ns which are slightly shorter than those of **2a**,**b**. The k_r and k_{nr} values of **5a**,**b** are calculated to be $2.9 \times 10^7 - 5.3 \times 10^7$ s^{-1} and $3.3 \times 10^7 - 7.9 \times 10^7$ s^{-1}, respectively, both of which are roughly comparable to those of **1a**,**b** and **2a**,**b**. In sharp contrast, **3a**,**b** and **4a**,**b** show remarkably short lifetimes of 0.97−2.61 ns (Figure 6), which give the values $k_r = 3.8 \times 10^7 - 7.3 \times 10^7$ s^{-1} and $k_{nr} = 34 \times 10^7 - 96 \times 10^7$ s^{-1}. Consequently, whereas compounds **3a**,**b**−**5a**,**b** show similar k_r values, the k_{nr} values of **3a**,**b** and **4a**,**b** are significantly larger than those of the corresponding **5a**,**b** by more than 1 order of magnitude in many cases. Thus, the extremely fast nonradiative processes occur in **3a**,**b** and **4a**,**b** as compared to **1a**,**b**, **2a**,**b**, and **5a**,**b**, which can be attributed to the internal conversion and/or intersystem crossing. The phosphorescence for **1b**−**5b** was observed in the region of about 600−800 nm at 77 K in 2-methyltetrahydrofuran, illustrating that the intersystem crossing in **1**−**5** is involved in the nonradiative processes (Figure 7 and Supplementary Figure 17−21).

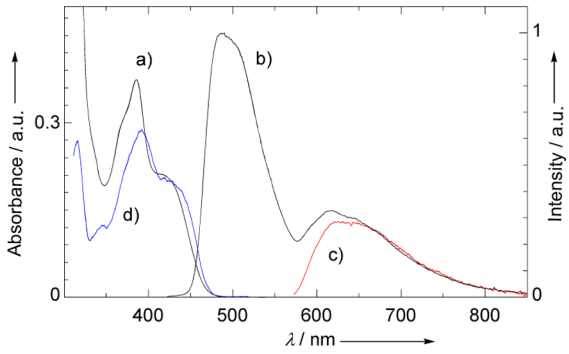

Figure 7. (a) UV−vis, (b) total emission, (c) phosphorescence, and (d) phosphorescence excitation (λ_{em} = 620 nm) spectra of **4b** in 2-methyltetrahydrofuran matrix at 77 K.

In order to determine the relative contribution of the internal conversion and intersystem crossing to the nonradiative energy dissipation, we performed time-resolved photoacoustic measurements for **1b**−**5b** in toluene at room temperature and estimated their quantum yields of intersystem crossing (Φ_{isc}).[32] The Φ_{isc} values of **1b**, **2b**, **3b**, **4b**, and **5b** are 0.26, 0.56, 0.94, 0.92, and 0.61, respectively. It is noteworthy that the sums of the Φ_f and Φ_{isc} values for **1b**−**5b** are almost equal to 1 within the experimental errors in all cases. Based on the equation $\Phi_f + \Phi_{isc} + \Phi_{ic} = 1$, where Φ_{ic} is the quantum yield of internal conversion, one can consider that the internal conversion hardly occurs in **1b**−**5b** and hence the k_{nr} values almost correspond to the k_{isc} values. Thus, the fast nonradiative processes for **3a**,**b** and **4a**,**b** are ascribed predominantly to the fast intersystem crossing. The heavy-atom effect of the sulfur atom in the BTD moiety may be one of the reasons for somewhat fast intersystem crossing to the triplet state in **1**−**5** (*vide infra*).

Electrochemistry. The electrochemical properties of **1a**−**c**, **2a**−**c**, and **3b**−**5b** were examined by cyclic voltammetry (CV; Table 2) in *o*-DCB (0.1 M *n*-Bu_4NPF_6, standard Fc^+/Fc), and

Table 2. Oxidation and Reduction Potentials of 1−5 by CV in *o*-DCB (0.1 M *n*-Bu_4NPF_6),[a] Theoretically Calculated HOMO and LUMO Levels,[b] and Optical Energy Gap

	E_{onset}^{ox} (E_{pa}) [V]	E_{onset}^{red} (E_{pc}) [V]	HOMO [eV]	LUMO [eV]	ΔE_{redox} [V][c]	ΔE_{opt} [eV][d]
1a	+0.23[f]	−2.19[e]			2.42	2.62
1b	+0.31[e]	−2.23[g]	−5.18	−2.00	2.54	2.54
	(+0.46)	(−2.42)				
1c	+0.39[e]	−2.24[g]			2.63	2.55
	(+0.51)	(−2.38)				
2a	+0.29[f]	−2.15[e]			2.44	2.69
2b	+0.40[h]	−2.25[g]	−5.24	−1.91	2.65	2.59
	(+0.59)	(−2.51)				
	(+1.12)					
2c	+0.44[g]	−2.25[e]			2.69	2.61
	(+0.59)	(−2.36)				
	(+1.01)					
3b	+0.62[e]	−2.22[g]	−5.52	−2.13	2.84	2.72
	(+0.77)	(−2.39)				
4b	+0.48[g]	−2.23[g]	−5.36	−2.04	2.71	2.63
	(+0.50)	(−2.48)				
5b	+0.26[g]	−2.22[h]	−5.06	−2.08	2.48	2.50
	(+0.42)	(−2.46)				
	(+0.86)					

[a]All potentials are given versus the Fc^+/Fc couple used as external standard. Scan rate: 100 mV s^{-1}. [b]B3LYP/6-311G**//B3LYP/6-31G*. [c]Electrochemical gap, ΔE_{redox}, is defined as the potential difference between E_{onset}^{ox} and E_{onset}^{red}. [d]Optical gap, ΔE_{opt}, is defined as the energy corresponding to the λ_{onset}, which is defined as the longest energy absorption wavelength with a molar absorptivity ε = 1000 M^{-1} cm^{-1} in CH_2Cl_2. [e]Irreversible wave. [f]Unresolved wave. [g]Reversible wave. [h]Quasi-reversible wave.

all of the compounds were found to display amphoteric behavior within the available potential window (Figure 8 and Supplementary Figure S22−S26, Supporting Information).[33] Compounds **1**−**5** exhibit a one BTD-centered $1e^-$ reduction step. The reduction onsets (E_{onset}^{red}) for **1**−**5** are observable in the region of −2.25 to −2.19 V, and the effect of the structural variation in **1**−**5** on the reduction potentials is insignificant. It is noted that their E_{onset}^{red} values are anodically shifted as compared to that for the parent BTD (−2.00 V). Thus, the reduction of **1**−**5** is clearly rendered more difficult by the effective conjugation with the strong thienopyrrole or indole donors. Whereas **1b**−**5b** and **1c** showed reversible or quasi-reversible waves, compounds **1a**, **2a**, and **2c** showed irreversible waves. This indicates that the functional groups on the nitrogen atoms in π-extended thiadiazoles play an important role in the

dx.doi.org/10.1021/jo301458m | J. Org. Chem. 2012, 77, 7595−7606

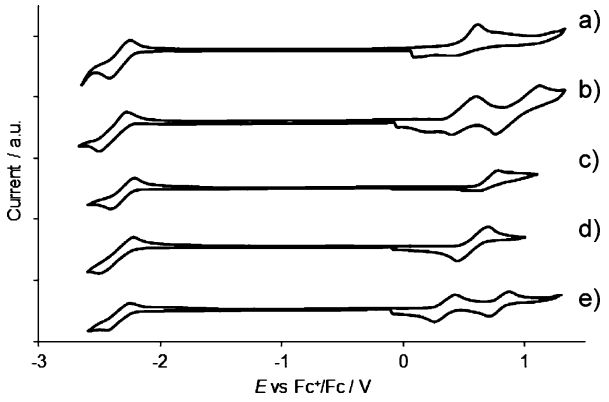

Figure 8. Cyclic voltammograms of (a) **1b**, (b) **2b**, (c) **3b**, (d) **4b**, and (e) **5b** measured in *o*-DCB (0.1 M n-Bu_4NPF_6) at a scan rate of 100 mV s^{-1}.

electrochemical stability and the ethyl groups more effectively stabilize the radical-anionic species than the benzyl groups.

Compounds **1a−c** and **2a−c** exhibited thienopyrrole-centered oxidation steps. Likewise, compounds **3b−5b** showed indole-centered oxidation steps. In sharp contrast to the reduction process, the potentials and the reversibility in the oxidation and back-oxidation processes are significantly dependent on the donor moieties. The oxidation onsets (E_{onset}^{ox}) for **1a−c** are cathodically shifted as compared to the corresponding **2a−c** by 50−90 mV. The oxidation peak amplitude of **1a** and **2a** was quite large after the first oxidation, indicative of their electrochemical polymerization and/or decomposition after the oxidation (Supplementary Figure S22 and S24, Supporting Information). Compounds **1b,c** also display irreversible thienopyrrole-centered oxidation waves, however, the isomeric compounds **2b,c** show different oxidation behavior from that of the corresponding **1b,c**. Thus, **2b** displays distinct, two $1e^-$ oxidation steps, and the first and second oxidation waves are quasi-reversible and irreversible, respectively. Compound **2c** having benzyl groups experienced two reversible $1e^-$ oxidation steps (Supplementary Figure S26). These results confirm that the orientation of the fused thiophene rings in **1** and **2** affects the kinetic stability of electrochemically generated cationic species. The E_{onset}^{ox} value of **3b** shifts anodically relative to those of **1b** and **2b** by 310 mV and 220 mV, respectively, clearly reflecting the difference of electron-donating ability between thiophene and benzene. Introduction of the electron-donating substituents in the indole moieties brings about the cathodic shifts of the E_{onset}^{ox} values (+0.62 V (**3b**), +0.48 V (**4b**), and +0.26 V (**5b**)), that is, the elevating of the HOMO levels. The Hammett σ_p values of *t*-Bu and OMe groups are −0.20 and −0.27, respectively,[34] and thus the observed trend for the E_{onset}^{ox} values follows the electron-donating ability of the substituents. The two well-separated, reversible $1e^-$ oxidation steps for **5b** were observable as in the case with **2b** and **2c**. The E_{onset}^{ox} value of +0.26 V for **5b** is more cathodic than those for **1b** and **2b** by 50 mV and 140 mV, respectively, and thus **5b** is found to possess the strongest donor ability in a series of **1b−5b**. The oxidation wave for **3b** was irreversible, while those for **4b** and **5b** were almost reversible. This suggests that the functional groups in the indole moieties in **4b** and **5b** play an important role in the stability of electrochemically generated cationic species as well as the donor ability.

Theoretical Calculations. We carried out the electronic transition analysis of **1b−5b** by time-dependent (TD) DFT at the B3LYP/6-31G* level of theory with the ground-state geometry optimized at the B3LYP/6-31G* level without any symmetry restriction (Supplementary Table S4−S8, Supporting Information). The absorption maxima in the low-energy region of **2b**, **4b**, and **5b** are related to the HOMO−LUMO transitions, whereas those of **1b** and **3b** are attributed to the weak transitions from the HOMO−LUMO+1 as well as the strong HOMO−LUMO transitions. The calculated λ_{max}^{abs} values are red-shifted with respect to the experimental values by 5−35 nm. The calculated λ_{max}^{abs} value (458 nm) of **1b** is longer than that of **2b** (441 nm), which compares well with the experimental data. The calculated λ_{max}^{abs} values of **3b**, **4b**, and **5b** are 425, 436, and 476 nm, respectively. Thus, **3b−5b** follow the observed trend for the λ_{max}^{abs} in the experiments, where the introduction of the functional groups in the indole moieties resulted in the more red-shifted absorption bands (Figure 2a).

The effects of the orientation of fused thiophene rings in **1b** and **2b** and the substituents in the indole moieties of **3b−5b** on their electronic structures were studied by molecular orbital calculations. The frontier molecular orbitals (FMOs) and the HOMO and LUMO levels of **1b−5b** were obtained by the single-point calculations at the B3LYP/6-311G**//B3LYP/6-31G* level of theory. The results are summarized in Table 2. The calculated HOMO levels of **1b** and **2b** are higher than that of **3b**, and the HOMO levels apparently rise from **3b**, **4b**, to **5b**. The LUMO levels of **1b−5b** are less changed than the HOMO levels. Thus, the calculated HOMO−LUMO gaps become smaller from **3b**, **2b**, to **1b**, and compound **5b** displays the smallest gap in the series of **1b−5b**. These findings qualitatively agree well with the results in the CV and UV−vis data. The HOMOs and LUMOs of **1b−5b** are shown in Figure 9. The HOMOs are delocalized over the whole π-system. The HOMO density of **1b** is found on the C=C bonds in the thiophene moieties similar to typical thiophene derivatives, whereas that of

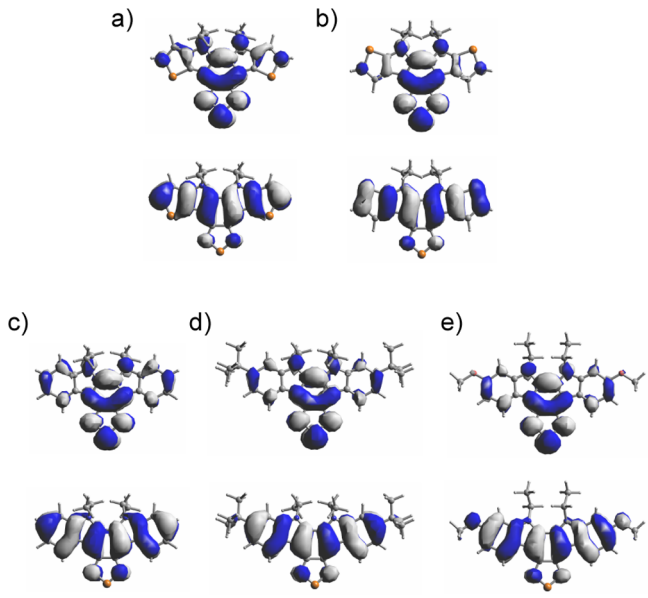

Figure 9. Molecular orbital plots of (a) **1b**, (b) **2b**, (c) **3b**, (d) **4b**, and (e) **5b** calculated by B3LYP/6-311G**//B3LYP/6-31G*. The upper plots represent the LUMOs, and the lower plots represent the HOMOs.

dx.doi.org/10.1021/jo301458m | J. Org. Chem. 2012, 77, 7595−7606

2b is found on the C−S bonds as well as the C=C bonds, which may be responsible for their different properties. The LUMOs of **1b**−**5b** have large contribution from the electron-accepting BTD moiety. This implies that the sulfur atom in the BTD moiety promotes triplet formation by intersystem crossing. The FMOs of **3b**−**5b** readily explain the reason why the introduction of the electron-donating substituents in **4b** and **5b** affects the oxidation potentials than the reduction potentials. The considerably larger HOMO densities than the LUMO densities in the indole moieties should lead to the destabilization of the HOMOs through the introduction of the electron-donating substituents. Indeed, the HOMO density of **5b** has substantial contribution from the OMe groups, whereas its LUMO has almost no contribution.

OFET Properties. We performed thermal gravimetric analysis (TGA) of **1b**−**5b**, which revealed that they are thermally stable up to *ca.* 300 °C (Supplementary Table S16, Supporting Information). Again, **1b**−**5b** can be readily sublimed at about 130 °C by using a high vacuum pump under laboratory conditions, which offers the potential for thin film preparation by vapor deposition techniques.[35] We became interested in the relationship between the solid-state structures of **1b** and **2b** and their semiconducting nature. On the basis of the crystal structures of **1b** and **2b**, we estimated the intermolecular transfer integrals (t) of the HOMOs and LUMOs between the neighboring molecules by Amsterdam density functional (ADF) calculations.[36,37] The calculations were independently performed for the HOMOs and LUMOs of the molecules. The calculated t values of the HOMOs are significantly larger than those of the LUMOs, and large transfer integral values of 151.4 and 102.7 meV for **1b** and **2b**, respectively, were observed along the π-stacked directions (a-axis (**1b**), b-axis (**2b**)) (Supplementary Table S14 and S15). This observation implies that efficient hole-transport along the a-axis and b-axis for **1b** and **2b**, respectively, is favorable. In the crystal structure of **2b**, the moderate t value of 27.0 meV was also observable in the a-axis, whereas the value in **1b** in the b-axis is almost negligible (6.4 meV), which indicates that the electronic structure of **1b** with a sheet-like network is more anisotropic than that of **2b**.

We carried out to fabricate OFET devices with a bottom-contact configuration with both **1b** and **2b** to evaluate the field-effect carrier mobility. At first, the thin films of **1b** and **2b** acting as the active layer were spin-coated from $CHCl_3$ solutions (1.0 wt %), and the electrical characteristics were measured under vacuum (10^{-2} Pa) at room temperature after annealing at 100 °C for 0.5 h. As expected from the high oxidation potentials of **1b** and **2b**, the devices exhibited the typical p-channel FET behavior and the n-channel behavior was not observed. The mobility of **1b**-based device was too low to be determined. The mobility of **2b**-based device was found to be 0.9×10^{-5} cm^2 V^{-1} s^{-1} with an on/off current ratio of 10^6 and a threshold of 13 V from the plot of the square root of the drain current versus the gate voltage. Next, the active layer was prepared by vapor deposition. The mobility of **1b**-based device was again too low to be estimated. The **2b**-based device showed the mobility of 2.7×10^{-5} cm^2 V^{-1} s^{-1}, which is better than that of the device prepared by a spin-coating method, with an on/off current ratio of 10^5 and a threshold voltage of 17 V (Figure 10).

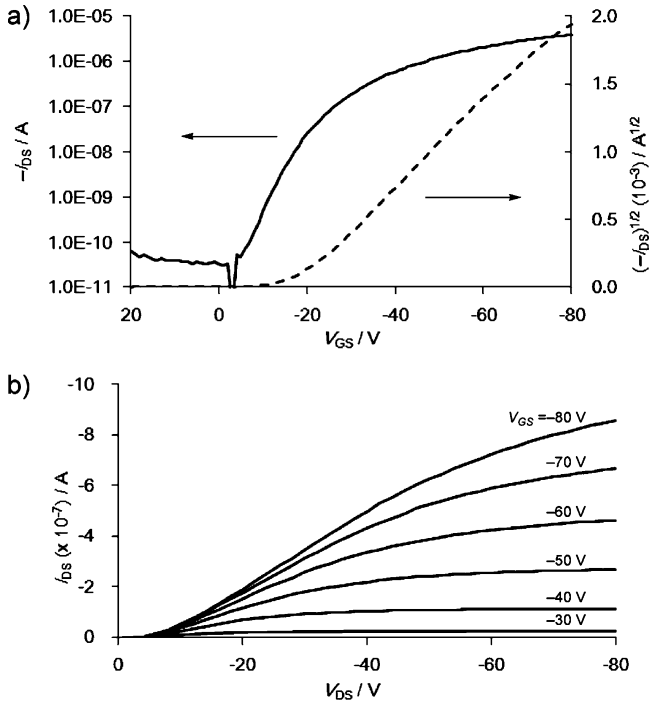

Figure 10. (a) Output and (b) transfer (V_{SD} = −80 V) characteristics of a **2b**-based OFET device prepared by vapor deposition. I_{SD}, V_{SD}, and V_{GS} denote source-drain current, source-drain voltage, and gate voltage, respectively.

CONCLUSION

In conclusion, we have synthesized π-extended thiadiazoles **1**−**5** fused with thienopyrrole or indole moieties by Stille cross-coupling reactions of **6** with the corresponding aryltin derivatives, followed by PPh_3-mediated reductive cyclization reactions as key steps. The X-ray crystallographic analyses of **1a**, **1b**, **2b**, **4a**, and **5b** revealed that they form the dense crystal packing and compounds **1a** and **4a** construct the unique supramolecular networks via multiple hydrogen bonding with water molecules. The electronic structure of **1**−**5** was approached by the UV−vis and fluorescence spectral measurements, CV, and DFT calculations. Their intramolecular CT interactions were clearly confirmed. The thienopyrrole-fused **1b** and **2b** display bathochromically shifted absorption spectra, namely small HOMO−LUMO gaps, and low oxidation potentials as compared to the indole-fused **3b**. The introduction of the *t*-Bu- and OMe-substituents in **4b** and **5b**, respectively, brings about the decrease of HOMO−LUMO gaps and the increase of donor ability. We have presented that the functional groups in the indole moieties dramatically affect the fluorescence behavior: **3b** and **4b** display significantly lower Φ_f values than **5b** due to the significantly fast intersystem crossing. Using thienopyrrole-fused compounds **1b** and **2b** as the active layer, we fabricated OFETs by vapor deposition and spin coating, and found that the orientation of the fused thiophene rings is an important factor in the device performance, which may reflect the difference of their packing structures as demonstrated by the X-ray diffraction analyses. We believe that the results in the present study provide the useful guideline to alter the photophysical and electrochemical properties and solid-state structures of π-extended thiadiazoles for their application into π-functional materials. Further structural functionalization of π-extended thiadiazoles is currently underway in our group.

dx.doi.org/10.1021/jo301458m | J. Org. Chem. 2012, 77, 7595−7606

EXPERIMENTAL SECTION

General Procedure of PPh_3-Mediated Reductive Cyclization for Preparation of π-Extended Thiadiazoles Fused with Thienopyrrole or Indole Moieties. A mixture of dinitro precursor (1 equiv) and PPh_3 (10 equiv) in *o*-DCB (~20 mM) was bubbled by argon for 15 min and stirred at 180 °C for 8−14 h. The mixture was cooled to room temperature, and the solvent was removed in vacuo. The residue was subjected to column chromatography and the collected material was subsequently washed with $CHCl_3$ or $CHCl_3$/hexane.

General Procedure for *N*-Ethylation. A mixture of π-extended thiadiazole derivatives (1 equiv), iodoethane (~6.5 equiv), and sodium hydroxide (~10 equiv) in DMF (~20 mM) was stirred at 50 °C for 2−6 h. After the mixture was poured into water, the resulting suspension was extracted with toluene/ethyl acetate (1:1). The combined organic phase was washed with water, and evaporated in vacuo after dried over anhydrous magnesium sulfate. The residue was purified by column chromatography.

Preparation of 1a.[21g] Compound **7** (735 mg, 1.88 mmol) was allowed to react with PPh_3 (4.92 g, 18.8 mmol) for 13 h according to the general procedure of PPh_3-mediated reductive cyclization. The crude product was subjected to column chromatography (silica gel; toluene/ethyl acetate 2:1) and the collected material was subsequently washed with $CHCl_3$ to give **1a** (598 mg, 1.82 mmol, 97%) as orange solids. Mp 137−139 °C; ^{1}H NMR (300 MHz, acetone-d_6): δ 11.23 (br s, 2H), 7.54 (d, J = 5.1 Hz, 2H), 7.31 (d, J = 5.1 Hz, 2H); ^{13}C NMR (150 MHz, acetone-d_6): δ 148.5, 142.3, 130.7, 127.4, 120.9, 113.1, 108.6; UV−vis (CH_2Cl_2): λ_{max} (ε) 265 (21400), 311 (26900), 325 (28700), 351 (15200), 423 (5800) nm; HR-FAB-MS (NBA, positive): m/z calcd for $C_{14}H_6N_4S_3^+$ 325.9755, found 325.9759 (M^+).

Preparation of 1b. Compound **1a** (50 mg, 0.15 mmol) was allowed to react with iodoethane (156 mg, 1.00 mmol) in the presence of sodium hydroxide (60 mg, 1.50 mmol) for 4 h according to the general procedure for *N*-ethylation. The crude product was purified by column chromatography (silica gel; toluene/hexane 10:1) to give **1b** (54 mg, 0.14 mmol, 95%) as brown solids. Mp 210−213 °C; ^{1}H NMR (300 MHz, $CDCl_3$): δ 7.46 (d, J = 5.1 Hz, 2H), 7.23 (d, J = 5.1 Hz, 2H), 4.56 (q, J = 7.2 Hz, 4H), 1.54 (t, J = 7.2 Hz, 6H); ^{13}C NMR (125 MHz, $CDCl_3$): δ 147.5, 145.6, 132.0, 127.1, 121.6, 111.7, 111.0, 45.0, 15.4; UV−vis (CH_2Cl_2): λ_{max} (ε) 263 (23300), 313 (31200), 330 (27700), 367 (19500), 436 (7100) nm; HR-FAB-MS (NBA, positive): m/z calcd for $C_{18}H_{14}N_4S_3^+$ 382.0381, found 382.0393 (M^+); Elemental analysis calcd (%) for $C_{18}H_{14}N_4S_3$: C 56.52, H 3.69, N 14.65; found C 56.37, H 3.61, N 14.46.

Preparation of 1c. A mixture of **1a** (40 mg, 0.12 mmol), benzyl bromide (98 mg, 0.57 mmol), and sodium hydroxide (49 mg, 1.23 mmol) in DMF (6 mL) was stirred at 60 °C for 10 h. After the mixture was poured into water (30 mL), the resulting suspension was extracted with toluene/ethyl acetate (1:1, 50 mL × 5). The combined organic phase was washed with water (100 mL × 3), and evaporated in vacuo after dried over anhydrous magnesium sulfate. The residue was purified by column chromatography (silica gel; toluene/hexane 5:1) to give **1c** (26 mg, 0.05 mmol, 43%) as pale orange solids. Mp 201−204 °C; ^{1}H NMR (300 MHz, $CDCl_3$): δ 7.34−7.26 (m, 8H), 6.98 (dd, J = 2.1 and 6.0 Hz, 4H), 6.77 (d, J = 5.1 Hz, 2H), 5.39 (s, 4H); ^{13}C NMR: Not available due to low solubility; UV−vis (CH_2Cl_2): λ_{max} (ε) 262 (19700), 313 (25700), 330 (23800), 366 (18900), 434 (6200) nm; HR-FAB-MS (NBA, positive): m/z calcd for $C_{28}H_{18}N_4S_3^+$ 506.0694, found 506.0693 (M^+).

Preparation of 2a. Compound **8** (302 mg, 0.77 mmol) was allowed to react with PPh_3 (2.09 g, 7.97 mmol) for 12 h according to the general procedure of PPh_3-mediated reductive cyclization. The crude product was subjected to column chromatography (silica gel; toluene/ethyl acetate 8:1) and the collected material was subsequently washed with $CHCl_3$ to give **2a** (231 mg, 0.71 mmol, 93%) as pale brown solids. Mp 115−118 °C; ^{1}H NMR (300 MHz, acetone-d_6): δ 11.40 (br s, 2H), 7.66 (d, J = 5.4 Hz, 2H), 7.24 (d, J = 5.4 Hz, 2H); ^{13}C NMR (150 MHz, acetone-d_6): δ 149.0, 138.7, 131.3, 128.3, 121.1, 118.6, 107.9; UV−vis (CH_2Cl_2): λ_{max} (ε) 274 (19300), 352 (12000), 415 (5100) nm; HR-FAB-MS (NBA, positive): m/z calcd for $C_{14}H_6N_4S_3^+$ 325.9755, found 325.9743 (M^+).

Preparation of 2b. Compound **2a** (432 mg, 1.32 mmol) was allowed to react with iodoethane (1.26 g, 8.05 mmol) in the presence of sodium hydroxide (531 mg, 13.3 mmol) for 7 h according to the general procedure for *N*-ethylation. The crude product was purified by column chromatography (silica gel; toluene) to give **2b** (370 mg, 0.97 mmol, 73%) as orange solids. Mp 187−190 °C; ^{1}H NMR (300 MHz, $CDCl_3$): δ 7.74 (d, J = 4.8 Hz, 2H), 7.14 (d, J = 4.8 Hz, 2H), 4.38 (q, J = 7.2 Hz, 4H), 1.62 (t, J = 7.2 Hz, 6H); ^{13}C NMR (125 MHz, $CDCl_3$): δ 148.0, 143.0, 133.0, 128.0, 120.6, 118.7, 110.3, 46.4, 14.4; UV−vis (CH_2Cl_2): λ_{max} (ε) 278 (22700), 366 (17200), 425 (7000) nm; HR-FAB-MS (NBA, positive): m/z calcd for $C_{18}H_{14}N_4S_3^+$ 382.0381, found 382.0378 (M^+); Elemental analysis calcd (%) for $C_{18}H_{14}N_4S_3$: C 56.52, H 3.69, N 14.65; found C 56.48, H 3.73, N 14.53.

Preparation of 2c. A mixture of **2a** (81 mg, 0.24 mmol), benzyl bromide (155 mg, 0.90 mmol), and sodium hydroxide (70 mg, 1.72 mmol) in DMF (12 mL) was stirred at 60 °C for 7 h. After the mixture was poured into water (30 mL), the resulting suspension was extracted with toluene/ethyl acetate (1:1, 50 mL × 5). The combined organic phase was washed with water (100 mL × 3), and evaporated in vacuo after dried over anhydrous magnesium sulfate. The residue was purified by column chromatography (silica gel; toluene) to give **2c** (38 mg, 0.07 mmol, 31%) as pale yellow solids. Mp 227−230 °C; ^{1}H NMR (300 MHz, $CDCl_3$): δ 7.78 (d, J = 5.4 Hz, 2H), 7.33−7.29 (m, 6H), 7.07 (d, J = 5.4 Hz, 2H), 7.03 (dd, J = 5.4 Hz, 2.1 and 3.6 Hz, 4H), 5.36 (s, 4H); ^{13}C NMR: Not available due to low solubility; UV−vis (CH_2Cl_2): λ_{max} (ε) 278 (21200), 365 (16600), 424 (6400) nm; HR-FAB-MS (NBA, positive): m/z calcd for $C_{28}H_{18}N_4S_3^+$ 506.0694, found 506.0691 (M^+).

Preparation of 3a.[21b] Compound **9** (50 mg, 0.13 mmol) was allowed to react with PPh_3 (347 mg, 13.2 mmol) for 12 h according to the general procedure of PPh_3-mediated reductive cyclization. The crude product was subjected to column chromatography (silica gel; toluene/ethyl acetate 8:1) and the collected material was subsequently washed with $CHCl_3$/hexane to give **3a** (38 mg, 0.12 mmol, 93%) as yellow solids: The ^{1}H NMR data are in agreement with those previously reported. ^{1}H NMR (300 MHz, acetone-d_6): δ 11.25 (br s, 2H), 8.61 (dd, J = 7.5 and 2.1 Hz, 2H), 7.75 (dd, J = 7.8 and 2.1 Hz, 2H), 7.45−7.38 (m, 4H).

Preparation of 3b. Compound **3a** (51 mg, 0.16 mmol) was allowed to react with iodoethane (148 mg, 0.95 mmol) in the presence of sodium hydroxide (51 mg, 1.27 mmol) for 2 h according to the general procedure for *N*-ethylation. The crude product was purified by column chromatography (silica gel; hexane/toluene 1:2) to give **3b** (51 mg, 0.14 mmol, 87%) as yellow solids. Mp 179−181 °C; ^{1}H NMR (300 MHz, $CDCl_3$): δ 8.76 (d, J = 6.9 Hz, 2H), 7.63 (d, J = 6.9 Hz, 2H), 7.54−7.44 (m, 4H), 4.66 (q, J = 7.2 Hz, 4H), 1.37 (t, J = 7.2 Hz, 6H); ^{13}C NMR (125 MHz, $CDCl_3$): δ 149.4, 141.8, 132.3, 126.0, 125.0, 122.4, 122.3, 112.9, 111.8, 43.4, 14.7; UV−vis (CH_2Cl_2): λ_{max} (ε) 273 (27000), 300 (27500), 312 (37500), 337 (7000), 387 (22600) nm; MALDI-TOF-MS (Dith, positive): m/z 370.09 (M^+); Elemental analysis calcd (%) for $C_{22}H_{18}N_4S$: C 71.32, H 4.90, N 15.12; found C 71.34, H 4.96, N 15.08.

Preparation of 4a. Compound **10** (152 mg, 0.31 mmol) was allowed to react with PPh_3 (1.00 g, 3.81 mmol) for 8 h according to the general procedure of PPh_3-mediated reductive cyclization. The crude product was subjected to column chromatography (silica gel; toluene) and the collected material was subsequently washed with $CHCl_3$/hexane to give **4a** (90 mg, 0.21 mmol, 70%) as yellow solids: Mp > 300 °C; ^{1}H NMR (300 MHz, acetone-d_6): δ 11.03 (br s, 2H), 8.50 (d, J = 8.4 Hz, 2H), 7.74 (d, J = 1.8 Hz, 2H), 7.53 (dd, J = 8.4 and 1.8 Hz, 2H), 1.45 (s, 18H); ^{13}C NMR (150 MHz, acetone-d_6): δ 150.1, 148.8, 139.5, 130.1, 122.9, 121.5, 120.4, 109.5, 109.2, 35.7, 32.1; UV−vis (CH_2Cl_2): λ_{max} (ε) 271 (33500), 299 (29700), 312 (46800), 368 (18400), 412 (10200) nm; HR-FAB-MS (NBA, positive): m/z calcd for $C_{26}H_{26}N_4S^+$ 426.1878, found 426.1894 (M^+).

Preparation of 4b. Compound **4a** (51 mg, 0.12 mmol) was allowed to react with iodoethane (115 mg, 0.74 mmol) in the presence

dx.doi.org/10.1021/jo301458m | J. Org. Chem. 2012, 77, 7595−7606

of sodium hydroxide (38 mg, 0.94 mmol) for 6 h according to the general procedure for *N*-ethylation. The crude product was purified by column chromatography (silica gel; hexane/toluene 1:3) to give **4b** (51 mg, 0.10 mmol, 90%) as yellow solids. Mp 200−204 °C; ^{1}H NMR (300 MHz, $CDCl_3$): δ 8.65 (d, J = 8.1 Hz, 2H), 7.64 (d, J = 1.2 Hz, 2H), 7.56 (dd, J = 8.1 and 1.2 Hz, 2H), 4.73 (q, J = 7.2 Hz, 4H), 1.50 (s, 18H), 1.37 (t, J = 7.2 Hz, 6H); ^{13}C NMR (125 MHz, $CDCl_3$): δ 149.4, 148.6, 142.0, 132.5, 123.9, 121.6, 120.6, 112.6, 108.1, 43.3, 35.4, 32.0, 14.6; UV−vis (CH_2Cl_2): λ_{max} (ε) 275 (28400), 303 (29400), 316 (42300), 335 (7200), 387 (19700) nm; HR-FAB-MS (NBA, positive): m/z calcd for $C_{30}H_{34}N_4S^+$ 482.2504, found 482.2502 (M^+).

Preparation of 5a.[21f] Compound **11** (101 mg, 0.23 mmol) was allowed to react with PPh_3 (707 mg, 2.69 mmol) for 14 h according to the general procedure of PPh_3-mediated reductive cyclization. The crude product was subjected to column chromatography (silica gel; toluene/ethyl acetate 4:1) and the collected material was subsequently washed with $CHCl_3$ to give **5a** (79 mg, 0.21 mmol, 92%) as orange solids. The ^{1}H NMR data are not included in the reported literature: Mp > 300 °C; ^{1}H NMR (300 MHz, acetone-d_6): δ 11.13 (br s, 2H), 8.44 (d, J = 8.7 Hz, 2H), 7.26 (d, J = 2.4 Hz, 2H), 7.06 (dd, J = 8.7 and 2.4 Hz, 2H), 3.92 (s, 6H); ^{13}C NMR: Not available due to low solubility; UV−vis (CH_2Cl_2): λ_{max} (relative intensity) 271 (0.71), 308 (0.63), 320 (1.0), 365 (0.41), 429 (0.23) nm; HR-FAB-MS (NBA, positive): m/z calcd for $C_{20}H_{14}N_4O_2S^+$ 374.0837, found 374.0837 (M^+).

Preparation of 5b. Compound **5a** (50 mg, 0.13 mmol) was allowed to react with iodoethane (126 mg, 0.80 mmol) in the presence of sodium hydroxide (44 mg, 1.07 mmol) for 6 h according to the general procedure for *N*-ethylation. The crude product was purified by column chromatography (silica gel; hexane/$CHCl_3$ 1:2) to give **5b** (44 mg, 0.10 mmol, 78%) as orange solids. An analytical sample for the elemental analysis was obtained by recrystallization from toluene. Mp 214−216 °C; ^{1}H NMR (300 MHz, $CDCl_3$): δ 8.59 (d, J = 8.7 Hz, 2H), 7.10 (s, 2H), 7.09 (d, J = 8.7, 2H), 4.63 (q, J = 7.2 Hz, 4H), 3.98 (s, 6H), 1.34 (t, J = 7.2 Hz, 6H); ^{13}C NMR (150 MHz, $CDCl_3$): δ 158.4, 149.2, 143.1, 132.1, 122.7, 120.4, 112.3, 110.8, 96.4, 56.0, 43.5, 14.5; UV−vis (CH_2Cl_2): λ_{max} (ε) 253 (46000), 277 (25100), 322 (36000), 384 (17600), 440 (10000) nm; HR-FAB-MS (NBA, positive): m/z calcd for $C_{24}H_{22}N_4O_2S^+$ 430.1463, found 430.1463 (M^+); Elemental analysis calcd (%) for $C_{24}H_{22}N_4O_2S$·0.1toluene (439.73): C 67.46, H 5.23, N 12.74; found C 67.31, H 5.30, N 12.57.

Preparation of 8. A mixture of **6** (406 mg, 1.05 mmol) and tributyl(3-thienyl)tin (948 mg, 2.53 mmol) in THF (14 mL) was bubbled with argon for 30 min. $Pd(PPh_3)_4$ (60 mg, 0.052 mmol) was added to the mixture. The mixture was heated at the refluxing temperature for 13 h, and the solvent was removed in vacuo. The residue was dissolved in CH_2Cl_2, and the resulting solution was filtered through a bed of silica gel. After the filtrate was evaporated in vacuo, the residue was subjected to column chromatography (silica gel; hexane/toluene 1:1) and the collected material was subsequently washed with hexane to give **8** (369 mg, 0.95 mmol, 87%) as yellow solids. Mp 254−255 °C; ^{1}H NMR (300 MHz, $CDCl_3$): δ 7.86 (dd, J = 3.0 and 1.5 Hz, 2H), 7.56 (dd, J = 5.0 and 3.0 Hz, 2H), 7.41 (dd, J = 5.0 and 1.5 Hz, 2H); ^{13}C NMR (150 MHz, $CDCl_3$): δ 152.8, 142.1, 129.6, 128.9, 127.9, 127.1, 123.4; UV−vis (CH_2Cl_2): λ_{max} (relative intensity) 298 (0.57), 396 (0.44) nm; HR-FAB-MS (NBA, positive): m/z calcd for $C_{14}H_6N_4O_4S_3^+$ 389.9551, found 389.9548 (M^+).

Preparation of 10. A mixture of **6** (153 mg, 0.38 mmol) and tributyl(4-*tert*-butylphenyl)tin (821 mg, 1.94 mmol) in THF (15 mL) was bubbled with argon for 15 min. $Pd(PPh_3)_4$ (23 mg, 0.020 mmol) was added to the mixture. The mixture was heated at refluxing temperature for 19 h, and the solvent was removed in vacuo. The residue was subjected to column chromatography (silica gel; hexane/toluene 2:3) and the collected material was subsequently washed with hexane to give **10** (165 mg, 0.38 mmol, 98%) as orange solids. Mp > 300 °C; ^{1}H NMR (300 MHz, $CDCl_3$): δ 7.58 (d, J = 8.7 Hz, 4H), 7.52 (d, J = 8.7 Hz, 4H), 1.40 (s, 18H); ^{13}C NMR (75 MHz, $CDCl_3$): δ 153.8, 153.2, 142.6, 129.0, 128.9, 127.6, 126.2, 35.1, 31.4; UV−vis (CH_2Cl_2): λ_{max} (ε) 295 (9000), 380 (7100) nm; HR-FAB-MS (NBA, positive): m/z calcd for $C_{26}H_{26}N_4O_4S^+$ 490.1675, found 490.1676 (M^+).

Preparation of 11.[21f] A mixture of **6** (201 mg, 0.516 mmol) and tributyl(4-methoxyphenyl)tin (511 mg, 1.28 mmol) in THF (12 mL) was bubbled with argon for 30 min. $Pd(PPh_3)_4$ (31 mg, 0.027 mmol) was added to the mixture. The mixture was heated at the refluxing temperature for 17 h, and the solvent was removed in vacuo. The residue was subjected to column chromatography (silica gel; toluene) and the collected material was subsequently washed with hexane to give **11** (148 mg, 0.395 mmol, 77%) as orange solids: ^{1}H NMR (300 MHz, $CDCl_3$): δ 7.53 (d, J = 9.0 Hz, 4H), 7.08 (d, J = 9.0 Hz, 4H), 3.90 (s, 6H); MALDI-TOF-MS (Dith, positive): m/z 438.01 (M^+).

Device Fabrication. The field-effect mobility was measured using bottom-contact thin-film field-effect transistor (FET) geometry. The n-doped silicon substrate functions as the gate electrode. A thermally grown silicon oxide (SiO_2) dielectric layer on the gate substrate has 300 nm thick and a capacitance of 10.0 nF cm^{-2}. Interdigital source and drain electrodes were constructed with gold (30 nm) that were formed on the SiO_2 layer. The channel width (W) and channel length (L) are 38 nm and 5 μm, respectively. The silicon oxide surface was first washed with acetone, water, and 2-propanol, and then activated by UV−ozone treatment. For the vacuum deposition, the substrate was pretreated with hexamethyldisilazane (HMDS) and washed with again with toluene, acetone, and 2-propanol. The semiconductor layer was vacuum deposited on the Si/SiO_2 at a rate of 1 Å/s under a pressure of 10^{-6} Pa to a thickness of 10 nm determined by a quartz crystal monitor or spin-coated from a solution in $CHCl_3$ (1.0 wt.%) at 1500 rpm for 1 min onto the substrate in air. The characteristics of the OFET devices were measured at room temperature under a pressure of 10^{-2} Pa without exposure by using a semiconductor parameter analyzer after the substrate was annealed at 100 °C for 30 min under a vacuum condition (10^{-2} Pa). The filed-effect mobility (μ) was calculated in the saturated region at the V_{SD} of −80 V by using the following equation. The current on/off ratio was determined from the I_{SD} at V_{GS} = 0 V (I_{off}) and V_{GS} = −80 V (I_{on}).

$$I_{SD} = WC_i\mu(V_{GS} - V_{th})^2/2L$$

■ ASSOCIATED CONTENT

Ⓢ Supporting Information

General experimental methods, X-ray data, cif files, UV−vis and fluorescence data, CV data, theoretical data, thermal gravimetric analysis data, and ^{1}H and ^{13}C NMR spectra of all new compounds. This material is available free of charge via the Internet at http://pubs.acs.org.

■ AUTHOR INFORMATION

Corresponding Author

*E-mail: nakamura@gunma-u.ac.jp. Tel: +81 277 30 1310. Fax: +81 277 30 1314.

Notes

The authors declare no competing financial interest.

■ ACKNOWLEDGMENTS

This work was supported by a Grant-in-Aid for Scientific Research from the Ministry of Education, Culture, Sports, Science and Technology, Japan, and performed under the Cooperative Research Program of "Network Joint Research Center for Materials and Devices" (Kyushu University, Osaka University). We thank Prof. Dr. Soichiro Kyushin (Gunma University) for generous permission to use an X-ray diffractometer, Prof. Dr. Teruo Shinmyozu (Kyushu University) for mass spectrometry measurements, and Dr. Mikio Yamasaki (Rigaku) for helpful suggestions for X-ray analyses.

REFERENCES

(1) (a) *Organic Electronics: Materials, Manufacturing and Applications*; Klauk, H., Eds.; Wiley-VCH: Weinheim, 2006. (b) *Organic Light Emitting Devices: Synthesis, Properties and Applications*; Müllen, K., Scherf, U., Eds.; Wiley-VCH: Weinheim, 2006. (c) *Functional Organic Materials*; Müller, T. J. J., Bunz, U. H. F., Eds.; Wiley-VCH: Weinheim, 2007. (d) *Organic Electroluminescence*; Kakafi, Z. H., Eds.; CRC Press: New York, 2005. (e) *Carbon-Rich Compounds: From Molecules to Materials*; Haley, M. M., Tykwinski, R. R., Eds.; Wiley-VCH: Weinheim, 2006.

(2) (a) Bao, Z.; Rogers, J. A.; Katz, H. E. *J. Mater. Chem.* **1999**, *9*, 1895−1904. (b) Kelley, T. W.; Baude, P. F.; Gerlach, C.; Ender, D. E.; Muyres, D.; Haase, M. A.; Vogel, D. E.; Theiss, S. D. *Chem. Mater.* **2004**, *16*, 4413−4422. Special issue on Organic Electronics and Optoelectronics: (c) Forrest, S. R., Thompson, M. E., Eds. *Chem. Rev.* **2007**, *107*, 923−1386. (d) Bendikov, M.; Wudl, F.; Perepichka, D. F. *Chem. Rev.* **2004**, *104*, 4891−4945. (e) Shirota, Y.; Kageyama, H. *Chem. Rev.* **2007**, *107*, 953−1010. (f) Wu, W.; Liu, Y.; Zhu, D. *Chem. Soc. Rev.* **2010**, *39*, 1489−1502.

(3) (a) Anthony, J. E. *Chem. Rev.* **2006**, *106*, 5028−5048. (b) Anthony, J. E. *Angew. Chem., Int. Ed.* **2008**, *47*, 452−483.

(4) (a) Grimsdale, A. C.; Müllen, K. *Angew. Chem., Int. Ed.* **2005**, *44*, 5592−5629. (b) Wu, J.; Pisula, W.; Müllen, K. *Chem. Rev.* **2007**, *107*, 718−747.

(5) (a) Takimiya, K.; Kunugi, Y.; Otsubo, T. *Chem. Lett.* **2007**, *107*, 578−583. (b) Takimiya, K.; Shimomura, S.; Osaka, I.; Miyazaki, E. *Adv. Mater.* **2011**, *23*, 4347−4370.

(6) Bunz, U. H. F. *Chem.—Eur. J.* **2009**, *15*, 6780−6789.

(7) Richards, G. J.; Hill, J. P.; Mori, T.; Ariga, K. *Org. Biomol. Chem.* **2011**, *9*, 5005−5017.

(8) Fukazawa, A.; Yamaguchi, S. *Chem. Asian J.* **2009**, *4*, 1386−1400 and references cited therein.

(9) For selected examples of ladder-type π-conjugated compounds incorporating nitrogen atom, see: (a) Patil, S. A.; Scherf, U.; Kadashchuk, A. *Adv. Funct. Mater.* **2003**, *13*, 609−614. (b) Bouchard, J.; Wakim, S.; Leclerc, M. *J. Org. Chem.* **2004**, *69*, 5705−5711. (c) Wu, Y.; Li, Y.; Gardner, S.; Ong, B. S. *J. Am. Chem. Soc.* **2005**, *127*, 614−618. (d) Boudreault, P.-L. T.; Wakim, S.; Blounin, N.; Simard, M.; Tessier, C.; Tao, Y.; Leclerc, M. *J. Am. Chem. Soc.* **2007**, *129*, 9125−9136. (e) Kawaguchi, K.; Nakano, K.; Nozaki, K. *J. Org. Chem.* **2007**, *72*, 5119−5128. (f) Kawaguchi, K.; Nakano, K.; Nozaki, K. *Org. Lett.* **2008**, *10*, 1199−1202. (g) Qi, T.; Guo, Y.; Liu, Y.; Xi, H.; Zhang, H.; Gao, X.; Liu, Y.; Lu, K.; Du, C.; Yu, G.; Zhu, D. *Chem. Commun.* **2008**, 6227−6229. (h) Balaji, G.; Phua, D. I.; Shim, W. L.; Valiyaveettil, S. *Org. Lett.* **2010**, *12*, 232−235. (i) Gao, P.; Cho, D.; Yang, X.; Enkelmann, V.; Baumgarten, M.; Müllen, K. *Chem.—Eur. J.* **2010**, *16*, 5119−5128. (j) Rajca, A.; Boratyński, P. J.; Olankitwanit, A.; Shiraishi, K.; Pink, M.; Rajca, S. *J. Org. Chem.* **2012**, *77*, 2107−2120.

(10) For selected examples of ladder-type π-conjugated compounds incorporating silicon atom, see: (a) Yamaguchi, S.; Xu, C.; Tamao, K. *J. Am. Chem. Soc.* **2003**, *125*, 13662−13663. (b) Xu, C.; Wakamiya, A.; Yamaguchi, S. *J. Am. Chem. Soc* **2005**, *127*, 1638−1639. (c) Matsuda, T.; Kadowaki, S.; Goya, T.; Murakami, M. *Org. Lett.* **2007**, *9*, 133−136. (d) Li, L.; Xiang, J.; Xu, C. *Org. Lett.* **2007**, *9*, 4877−4879.

(11) For selected examples of ladder-type π-conjugated compounds incorporating boron atom, see: (a) Agou, T.; Kobayashi, J.; Kawashima, T. *Org. Lett.* **2006**, *8*, 2241−2244. (b) Agou, T.; Kobayashi, J.; Kawashima, T. *Chem.—Eur. J.* **2007**, *13*, 8051−8090. (c) Chen, J.; Kampf, J. W.; Ashe, A. J., III *Organometallics* **2008**, *27*, 3639−3641. (d) Mercier, L. G.; Piers, W. E.; Parvez, M. *Angew. Chem., Int. Ed.* **2009**, *48*, 6108−6111. (e) Wood, T. K.; Piers, W. E.; B. Keay, A.; Parvez, M. *Chem.—Eur. J.* **2010**, *16*, 12199−12206. (f) Caruso, A., Jr.; Siegler, M.; Tovar, J. D. *Angew. Chem., Int. Ed.* **2010**, *49*, 4213−4217. (g) Hatakeyama, T.; Hashimoto, S.; Seki, S.; Nakamura, M. *J. Am. Chem. Soc.* **2011**, *133*, 18614−18617. (h) Iida, A.; Yamaguchi, S. *J. Am. Chem. Soc.* **2011**, *133*, 6952−6955. (i) Zhou, A.; Wakamiya, A.; Kushida, T.; Yamaguchi, S. *J. Am. Chem. Soc.* **2012**, *134*, 4529−4532.

(12) (a) Gompper, R.; Wagner, H.-U. *Angew. Chem., Int. Ed. Engl.* **1988**, *27*, 1437−1455. (b) Meier, H. *Angew. Chem., Int. Ed.* **2005**, *44*, 2482−2506.

(13) For recent reviews, see: (a) Kivala, M.; Diederich, F. *Acc. Chem. Res.* **2009**, *42*, 235−248. (b) Zucchero, A. J.; Mcgrier, P. L.; Bunz, U. H. F. *Acc. Chem. Res.* **2010**, *43*, 397−408. (c) Kato, S.-i.; Diederich, F. *Chem. Commun.* **2010**, *46*, 1994−2006. (d) Delgado, J. L.; Bouit, P.-A.; Filippone, S.; Herranz, Á.; Martín, N. *Chem. Commun.* **2010**, *46*, 4853−4865. (e) Beaujuge, P. M.; Fréchet, J. M. J. *J. Am. Chem. Soc.* **2011**, *133*, 20009−20029.

(14) (a) Naraso, Nishida, J.-i.; Ando, S.; Yamaguchi, J.; Itaka, K.; Koinuma, H.; Tada, H.; Tokito, S.; Yamashita, Y. *J. Am. Chem. Soc.* **2005**, *127*, 10142−10143. (b) Naraso, Nishida, J.-i.; Kumaki, D.; Tokito, S.; Yamashita, Y. *J. Am. Chem. Soc.* **2006**, *128*, 9598−9599.

(15) (a) Jia, C.; Liu, S.-X.; Tanner, C.; Leiggener, C.; Sanguinet, L.; Levillain, E.; Leutwyler, S.; Hauser, A.; Decurtins, S. *Chem. Commun.* **2006**, 1878−1880. (b) Guégano, X.; Kanibolotsky, A. L.; Blum, C.; Mertens, S. F. L.; Liu, S.-X.; Neels, A.; Hagemann, H.; Skabara, P. J.; Leutwyler, S.; Wandlowski, T.; Hauser, A.; Decurtins, S. *Chem.—Eur. J.* **2009**, *15*, 63−66. (c) Jia, H.-P.; Ding, J.; Ran, Y.-F.; Liu, S.-X.; Blum, C.; Petkova, I.; Hauser, A.; Decurtins, S. *Chem. Asian J.* **2011**, *6*, 3312−3321. (d) Jaggi, M.; Blum, C.; Marti, B. S.; Liu, S.-X.; Leutwyler, S.; Decurtins, S. *Org. Lett.* **2010**, *12*, 1344−1347.

(16) Yang, Y.; Wang, Y.; Xie, Y.; Xiong, T.; Yuan, Z.; Zhang, Y.; Qian, S.; Xiao, Y. *Chem. Commun.* **2011**, *47*, 10749−10751.

(17) Seillan, C.; Brisset, H.; Siri, O. *Org. Lett.* **2008**, *10*, 4013−4016.

(18) Tang, Q.; Liu, J.; Chan, H. S.; Miao, Q. *Chem.—Eur. J.* **2009**, *15*, 3965−3969.

(19) Chen, J.; Cao, Y. *Acc. Chem. Res.* **2009**, *42*, 1709−1718 and references cited therein.

(20) (a) Van Mullekom, H. A. M.; Vekemans, J. A. J. M.; Meijer, E. W. *Chem.—Eur. J.* **1998**, *4*, 1235−1243. (b) Brabec, C. J.; Winder, C.; Sariciftci, N. S.; Hummelen, J. C.; Dhanabalan, A.; Hal, P. A. V.; Janssen, R. A. J. *Adv. Funct. Mater.* **2002**, *12*, 709−712. (c) Jayakannan, M.; Hal, P. A. V.; Janssen, R. A. J. *J. Polym. Sci., Part A* **2002**, *40*, 2360−2372. (d) Zhang, F.; Jespersen, K. G.; Björström, C.; Svensson, M.; Andersson, M. R.; Sundström, V.; Magnusson, K.; Moons, E.; Yartsev, A.; Inganäs, O. *Adv. Funct. Mater.* **2006**, *16*, 667−674. (e) Bundgaard, E.; Krebs, F. C. *Sol. Energy Mater. Sol. Cells* **2007**, *91*, 954−985. (f) Durben, S.; Nickel, D.; Krüger, R. A.; Sutherland, T. C.; Baumgartner, T. *J. Polym. Sci., Part A* **2008**, *46*, 8179−8190. (g) Lu, J.; Liang, F.; Drolet, N.; Ding, J.; Tao, Y.; Movileanu, R. *Chem. Commun.* **2008**, 5315−5317. (h) Steinberger, S.; Mishra, A.; Reinold, E.; Müller, C. M.; Uhrich, C.; Pfeiffer, M.; Bäuerle, P. *Org. Lett.* **2011**, *13*, 90−93.

(21) For π-extended thiadiazoles, see: (a) Appleton, A. L.; Miao, S.; Brombosz, S. M.; Berger, N. J.; Barlow, S.; Marder, S. R.; Laurence, B. M.; Hardcastle, K. I.; Bunz, U. H. F. *Org. Lett.* **2009**, *11*, 5222−5225. (b) Balaji, G.; Shim, W. L.; Parameswaran, M.; Valiyaveettil, S. *Org. Lett.* **2009**, *11*, 4450−4453. (c) Linder, T.; Sutherland, T.; Baumgartner, T. *Chem.—Eur. J.* **2010**, *16*, 7101−7105. (d) Linder, T.; Badiola, E.; Baumgartner, T.; Sutherland, T. C. *Org. Lett.* **2010**, *12*, 4520−4523. (e) Lei, T.; Zhou, Y.; Cheng, C.-Y.; Cao, Y.; Peng, Y.; Bian, J.; Pei, J. *Org. Lett.* **2011**, *13*, 2642−2645. (f) Biniek, L.; Bulut, I.; Lévêque, P.; Heiser, T.; Leclerc, N. *Tetrahedron Lett.* **2011**, *52*, 1811−1814. (g) Cheng, Y.-S.; Chen, C.-H.; Ho, Y.-J.; Chang, S.-W.; Witek, H. A.; Hsu, C.-S. *Org. Lett.* **2011**, *13*, 5484−5487.

(22) Cheng and Hsu have reported the synthesis of **1a** by reductive cyclization of **7** with $P(OEt)_3$.[21g] We have presented the preparation of **1a−c** and **2a** at the 91th Annual Meeting of the Chemical Society of Japan, Yokohama, 2011; 1PC066.

(23) Zoombelt, A. P.; Fonrodona, M.; Turbiez, M. G. R.; Wienk, M. M.; Janssen, R. A. J. *J. Mater. Chem.* **2009**, *19*, 5336−5342.

(24) (a) Cadogan, J. I. G. *Organophosphorous Reagents in Organic Synthesis*; Academic Press: London, 1979; Chapter 6. (b) Freeman, A. W.; Urvoy, M.; Criswell, M. E. *J. Org. Chem.* **2005**, *70*, 5014−5019.

(25) Frisch, M. J.; Trucks, G. W.; Schlegel, H. B.; Scuseria, G. E.; Robb, M. A.; Cheeseman, J. R.; Montgomery, J. A., Jr.; Vreven, T.; Kudin, K. N.; Burant, J. C.; Millam, J. M.; Iyengar, S. S.; Tomasi, J.;

Barone, V.; Mennucci, B.; Cossi, M.; Scalmani, G.; Rega, N.; Petersson, G. A.; Nakatsuji, H.; Hada, M.; Ehara, M.; Toyota, K.; Fukuda, R.; Hasegawa, J.; Ishida, M.; Nakajima, T.; Honda, Y.; Kitao, O.; Nakai, H.; Klene, M.; Li, X.; Knox, J. E.; Hratchian, H. P.; Cross, J. B.; Bakken, V.; Adamo, C.; Jaramillo, J.; Gomperts, R.; Stratmann, R. E.; Yazyev, O.; Austin, A. J.; Cammi, R.; Pomelli, C.; Ochterski, J. W.; Ayala, P. Y.; Morokuma, K.; Voth, G. A.; Salvador, P.; Dannenberg, J. J.; Zakrzewski, V. G.; Dapprich, S.; Daniels, A. D.; Strain, M. C.; Farkas, O.; Malick, D. K.; Rabuck, A. D.; Raghavachari, K.; Foresman, J. B.; Ortiz, J. V.; Cui, Q.; Baboul, A. G.; Clifford, S.; Cioslowski, J.; Stefanov, B. B.; Liu, G.; Liashenko, A.; Piskorz, P.; Komaromi, I.; Martin, R. L.; Fox, D. J.; Keith, T.; Al-Laham, M. A.; Peng, C. Y.; Nanayakkara, A.; Challacombe, M.; Gill, P. M. W.; Johnson, B.; Chen, W.; Wong, M. W.; Gonzalez, C.; Pople, J. A. *Gaussian 03*, revision C.02; Gaussian, Inc.: Wallingford, CT, 2004.

(26) The cross-conjugative pathways in **2a**–**c** may also affect the spectral difference.

(27) The fluorescence spectra were recorded in the dilute regime (10^{-5}–10^{-6} M).

(28) The $E_T(30)$ parameters (33.9 kcal/mol for toluene, 37.4 kcal/mol for THF, 38.1 kcal/mol for EtOAc, 40.7 kcal/mol for CH_2Cl_2, 42.9 kcal/mol for DMF) are taken from: Reichardt, C. *Chem. Rev.* **1994**, *94*, 2319–2358.

(29) Suzuki, K.; Kobayashi, A.; Kaneko, S.; Takehira, K.; Yoshihara, T.; Ishida, H.; Shiina, Y.; Oishi, S.; Tobita, S. *Phys. Chem. Chem. Phys.* **2009**, *11*, 9850–9860.

(30) The solubility of **5a** in common organic solvents is insufficient to determine its molar absorptivity.

(31) The emission decay profiles were numerically fitted by single exponential kinetics.

(32) Kobayashi, A.; Takehira, K.; Yoshihara, T.; Uchiyama, S.; Tobita, S. *Photochem. Photobiol. Sci.* **2012**, *11*, 1368–1376.

(33) The CV for **3a**–**5a** was not performed, because their radical-cationic and -anionic species were expected to be unstable on the basis of the results for **1a** and **2a**.

(34) Hansch, C.; Leo, A.; Taft, R. W. *Chem. Rev.* **1991**, *91*, 165–195.

(35) The sublimation of **1a**, **1c**, **2a**, **2c**, **3a**, **4a**, and **5a** was not investigated.

(36) ADF2010.01; SCM, Theoretical Chemistry, Vrije Universiteit: Amsterdam, The Netherlands; http://www.scm.com.

(37) (a) Senthilkumar, K.; Grozema, F. C.; Bickelhaupt, F. M.; Siebbeles, L. D. A. *J. Chem. Phys.* **2003**, *119*, 9809–9817. (b) Prins, P.; Senthikumar, K.; Grozema, F. C.; Jonkheijm, P.; Schenning, A. P. H. J.; Meijer, E. W.; Siebbeles, L. D. A. *J. Phys. Chem. B* **2005**, *109*, 18267–18274.